(Received 27 November 2025, Accepted 23 December 2025, Scheduled 30 January 2026)

Design, Fabrication, and Evaluation of a Dual-Band Linearly Polarized Lamp-Shaped Wearable Antenna for ISM and Public Safety Bands

Shiv K. Singh[1], Atul Varshney[1,2], Tanuj Garg[1], Zahriladha Zakaria[3], and Ahmed J. A. Al-Gburi[3,*]

[1]*ECE Department, FET, Gurukula Kangri (Deemed to be) University, Haridwar 249404, Uttarakhand, India*
[2]*ECE Department, FET, Graphic Era (Deemed to be) University, Dehradun 249002, Uttarakhand, India*
[3]*Center for Telecommunication Research & Innovation (CeTRI)*
Fakulti Teknologi Dan Kejuruteraan Elektronik Dan Komputer (FTKEK)
Universiti Teknikal Malaysia Melaka (UTeM), Jalan Hang Tuah Jaya, 76100 Durian Tunggal, Melaka, Malaysia

ABSTRACT: This article describes a linearly polarized lamp-shaped dual-wideband monopole wearable antenna for use in Industrial, Scientific, and Medical (ISM), and public safety bands. To compress the antenna, the low current corners of the rectangular patch and the two regular octagons were eliminated. The lamp-shaped antenna of size $0.438\lambda_0 \times 0.449\lambda_0$ ($53.9 \times 55 \times 1.0\,\text{mm}^3$) was engraved on a jeans substrate at a frequency of 2.45 GHz. The antenna is 37.15% smaller (miniaturized) than a traditional rectangular patch antenna (59.7 mm × 78.68 mm) at the same design frequency. The antenna achieves dual widebands (2.17–2.86 GHz) and (4.42–5.06 GHz) with resonance frequencies of 2.45 and 4.70 GHz. At these resonant frequencies, the proposed wearable antenna has gain values of 3.86 dBi and 6.63 dBi and radiation efficiencies of 96.34% and 92.27%. Both the E- and H-planes exhibit bidirectional radiation characteristics. Thus, the proposed wearable antenna is the best for ISM, Wi-Fi, WLAN, Bluetooth, Wi-MAX (2.3 GHz), commercial, governmental, and military applications (4.40–4.99 GHz), hilly and watery rescue operations, radio astronomy services (4.80–4.94 GHz), public safety applications (4.94–4.99 GHz), Internet of Things (IoT), military fixed and mobile communications (4.40 to 4.50 GHz), and telemetry applications such as unmanned vehicles and drones. Finally, the detailed electrical equivalent circuit modelling and ON-body and OFF-body Specific Absorption Rate (SAR) investigations of the antenna are presented. The SAR values are found within the acceptable limits below 1.6 W/kg for 1 g of tissue.

1. INTRODUCTION

In the modern era, with the expansion of textile technology, the demand for smart wearable antennas has increased. Wearable antennas are prototyped on textile and non-textile materials. Textile antennas are widely used and have become much trendier nowadays, primarily in body-worn applications for health-parameter screening. The fabrication of these materials is made easy by the current state of the microstrip technology. The other advantages of wearable antennas include their cost-effectiveness, small size, light weight, ease of wear, lack of maintenance, simple fabrication, and easy installation. Certain professions, such as those in the medical, military, and firefighting fields, rely on body-centric communication systems. Furthermore, athletes, astronauts, and patients may benefit from wearing antennas for monitoring purposes. Therefore, there is increasing interest in studying wearable technology [1–5]. In the earlier period, researchers conducted many studies on button antennas [6], electro-textile antennas [7], and radio frequency (RF) antennas using wearable magnetic composite materials [8]. Some research has focused on antenna size miniaturization [9], while others have focused on antenna bending effects [10]. The vast array of Wi-Fi uses necessitates antenna compression for both transmitting and receiving signals, which in turn allows for more space inside the device and greater bandwidth [11]. Increased miniaturization of antennas is necessary to achieve the global maintenance of small wireless items. An ISM band patch antenna, with a resonance frequency of 2.45 GHz, is used by most small devices for short-distance communications [12, 13]. By employing a highly conductive polymer–graphene antenna for wearable applications operating at 2.45 GHz, as suggested in [14], the antenna exhibits a low SAR of 1.2 W/kg averaged over 10 g of tissue, thereby affirming the safety of integrating the proposed flexible graphene antenna into wearable devices. On the other hand, in order to attain high gain for amateur radio applications in the S-band, an array of four-element rectangular patches was designed [15]. A wearable wideband textile coplanar Vivaldi antenna for medical and IoT applications was proposed by Nurhayati et al. [16], exhibiting a wide operating bandwidth from 2.6 GHz to 8.7 GHz with a fractional bandwidth of up to 107%. Several planar and reconfigurable antennas operating at 2.45 GHz have been built and analyzed by Varshney et al. [17–19] for the use in applications including the ISM and PCS bands. Purohit and Raval devised a wearable rectangular patch monopole antenna. The antenna is 120 mm × 120 mm ×1.6 mm and has a high gain of

* Corresponding author: Ahmed Jamal Abdullah Al-Gburi (ahmedjamal@utem.edu.my, ahmedjamal@ieee.org).

9.41 dBi and a low −10 dB fractional bandwidth (FBW) [20]. Wang and Li proposed a double-band coaxial-fed wearable microstrip antenna on a denim cotton substrate. The same antenna worked at two frequencies: 2.45 GHz and 5.8 GHz (ISM). The antenna obtains gains of 8.49 dBi and 6.85 dBi at two resonance frequencies, respectively, with a smaller antenna overall size; nevertheless, the substrate thickness is 1.6 mm [21]. Zerith and Nesasudha proposed an edge-fed, meandering, rectangle-shaped monopole wearable antenna with a miniaturized size on a 1.0 mm thick polydimethylsiloxane (PDMS) substrate. The reduced substrate thickness reduces the antenna gain to 4.04 dBi while increasing the antenna radiation efficiency to 92% and narrowing the −10 dB FBW [22].

The Federal Communications Commission (FCC) in the United States and the European Telecommunications Standards Institute (ETSI) in Europe govern the 4.9 GHz public safety band, giving public safety entities priority access and sharing with non-traditional entities. The FCC approved 50 MHz of spectrum for fixed and mobile services with a licensing freeze and Band Manager control. Public safety agencies have priority access; sharing arrangements must avoid interference. Rules ensure optimal spectrum utilization for public safety communications. These regulations aim to optimize public safety communications and facilitate the integration of the latest technologies, including 5G. According to the literature, the majority of wearable antennas are single-band and focus solely on ISM band activities. None of the available research includes the commercial, governmental, and military applications (4.40–4.99 GHz), the public safety band (PSB) from 4.94 GHz to 4.99 GHz, and the ISM band (2.4–2.5 GHz) at the same time. The solution to this research gap is to create a dual-band antenna. The accessible pieces were created on a jeans substrate or a semi-flexible RO3003 substrate with varying thicknesses. The change in thickness produces/suppresses surface waves, while the change in substrate permittivity causes variations in the −10 dB FBW and antenna gain. As a result, it is difficult to attain a higher gain and a broader −10 dB FBW with lower permittivity and a thinner antenna.

The main aim of this study is to design a monopole wearable antenna at 2.45 GHz for the ISM band. Further, the authors explored the same antenna to achieve wideband with an acceptable gain above 3 dBi with a jeans substrate of thickness 1.0 mm, and to miniaturize the size of the antenna by more than 35% of its conventional size. Furthermore, this study aims to explore the same antenna for public safety band (4.94–4.99 GHz) and military applications (4.40–4.99 GHz) [23]. Another aim of this study is to investigate the antenna at its equivalent RLC circuit level, and the final aim of this antenna is to estimate the SAR for human phantoms in ON-body and OFF-body cases.

The quasi-fractal method helps to create the antenna's dual bands [24]. In this study, a unique wearable antenna structure was constructed using corner and octagon notches at the borders of a rectangular patch antenna to remove the low-current region from the patch and to change the surface current distribution in the newly formed lamp-shaped antenna structure. Corner and octagon cuts in the conducting patch increase the electrical length of the antenna. After patch corner and length truncation, the antenna behavior changed to a dual-band. The 4.70 GHz was not the targeted frequency, while the antenna achieved a bandwidth of 4.42–5.06 GHz in its upper band. This makes the antenna suitable for military applications (4.40–4.99 GHz) and public safety applications (4940–4990 MHz). The antenna's dual-wideband nature gave a new feature to the ISM band antenna, allowing it to be used for public safety bands and military applications.

A novel lamp-shaped antenna based on the quasi-fractal principle combines fractal cuts with rectangular patches to boost the electrical length of dual bands for ISM, military, and public safety. Corner truncation and octagonal cuts are based on low-current-area reduction. The capacitive impact is reduced by shortening the antenna ground length (making the antenna monopole), which reduces the patch current density magnitude and concentrates most of the current across the feed section and patch upper edge. The suggested SAR of the wearable antenna is below 1.6 W/kg for 1 g of tissue. The antenna was 37.15% smaller than traditional antennas. The low-SAR values in the ON-body and OFF-body cases remain below the regulatory limits specified by the DoT (Department of Telecommunications, India) and the International Commission on Non-Ionizing Radiation Protection (ICNIRP), where the SAR limit is 1.6 W/kg for 1 g of human tissue at distances less than 5 mm from the body phantom [25].

This article describes the design, optimization, and fabrication of a miniaturized, economical, and easy-to-fabricate monopole wearable antenna for ISM and public safety band applications. This study includes the antenna geometry with reflection coefficients, radiation patterns, gain, and axial ratio plots of the antenna.

2. METHODS AND MATERIALS

The suggested wearable antenna is 53.9 mm × 55 mm and is built on a low-profile jeans substrate. It has a permittivity of 1.6, thickness of 1.0 mm, and loss tangent of 0.05. The substrate properties, permittivity, and loss tangent measurements are described in Section 3.2. The design frequency is 2.45 GHz.

2.1. Antenna Design Development

The antenna evolved from conventional rectangular microstrip patch antenna (RPA) design equations [20, 26, 27]. The conventional RPA dimensions evaluated at design frequency 2.45 GHz are 53.70 mm and 47.68 mm with the full bottom surface of jeans ($\varepsilon_r = 1.6$, and $\tan\delta = 0.05$) substrate as ground when a copper layer is present on its whole surface, as shown in Step 1. In Step 2, the feed was inserted 5 mm inside the patch, and the corresponding substrate and ground lengths were reduced by 5 mm. In Step 3 and Step 4, the red and green colored areas were removed from the patch as low current magnitude distributions at the corner areas of the rectangular patch, as shown in Fig. 1. This leads to Step 5. Further, in Step 6, two symmetrical octagons centered at the corner of the Step 5 patch are removed, yielding the patch geometry in Step 7. Subsequently, the feed length is further reduced to 8.0 mm as shown in Step 8.

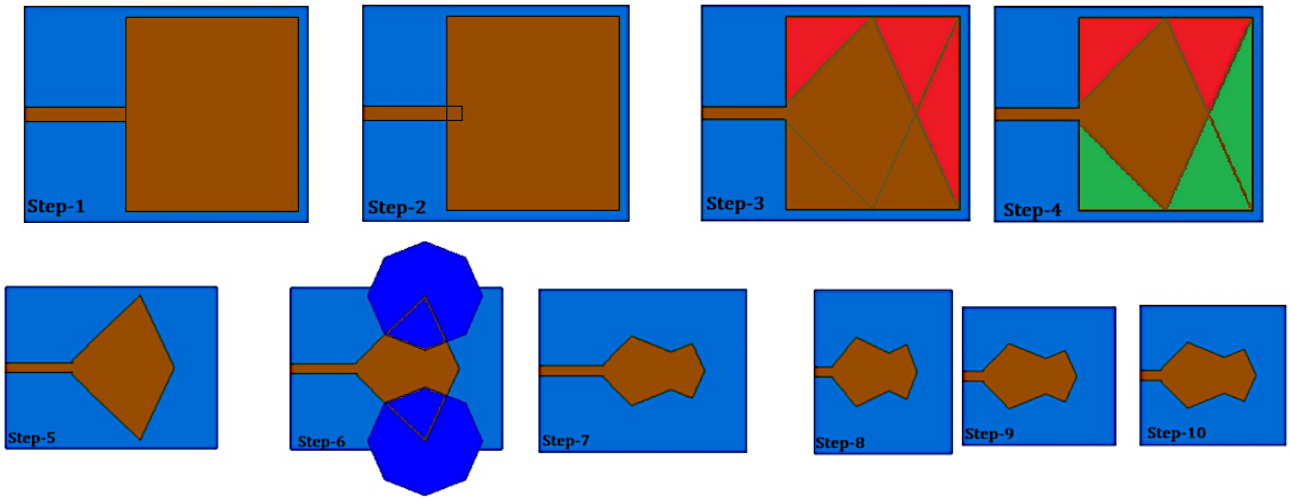

FIGURE 1. Antenna patch development to lamp-shaped wearable antenna geometry.

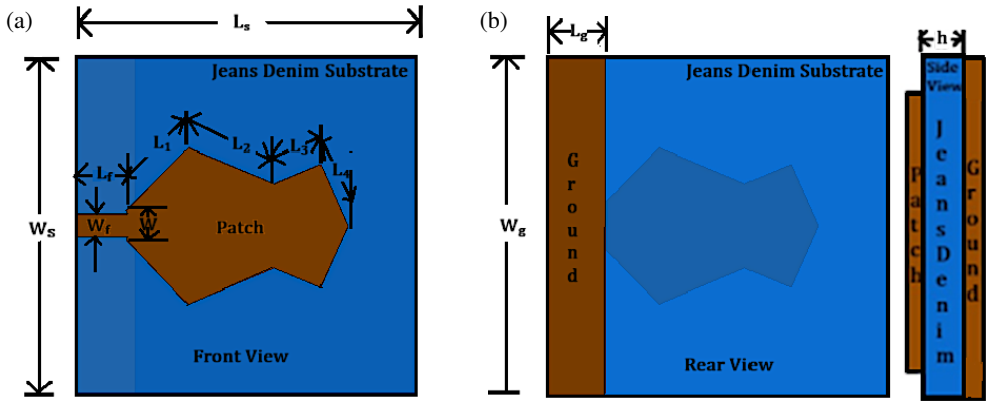

FIGURE 2. Lamp-shaped antenna dimensions representation. (a) Front view, (b) rear view, and (c) side view.

TABLE 1. Antenna dimensions scales.

Parameter	Designation	Values (in mm)
Substrate (Jeans) $\varepsilon_r = 1.6$	$W_S \times L_S \times h$	$53.9 \times 55 \times 1.0$
Ground (Copper)	$W_g \times L_g$ Thickness: t	53.9×9.43 0.035
Patch (Copper)	$W_P \times L_P$ Thickness: t	53.7×47.68 0.035
50 Ω Feed line	$W_f \times L_f$	3.75×8.0
Miscellaneous Dimensions	W, L_1, L_2, L_3, L_4	5.0, 14.1636, 15.08, 8.118, 10.8936

Furthermore, the antenna size was reduced by compressing the substrate and ground along its width and length, resulting in Steps 9 and 10. Fig. 1 shows all patch-creation phases. Subsequently, the ground length of the antenna is reduced towards the feed. When the ground length is 9.43 mm, the optimal reflection coefficient values are attained with dual-band performance. Figs. 2(a)–(c) show the final drawing of the front, back, and side perspectives of the antenna structure with optimized design parameters, and Table 1 displays all the specifications.

2.2. Binary Operations or Patch Structure Development

Initially, a standard patch antenna with a 28 mm feed length and a full bottom ground yields two narrow bands below −10 dB, with a peak gain of 2.63 dBi at the design frequency of 2.45 GHz. Subsequently, the 5 mm feed length is shortened, as the overall length of the substrate, and the ground is reduced to 5.0 mm, as illustrated in Step 2 of Fig. 1. This led to an increase in the gain and lower reflection coefficient values at the two resonant frequencies. After this step, the four triangular

TABLE 2. Effect of binary operations.

Rectangular-Cut	Tuning Freq. f_r (GHz)	S_{11} (dB)	−10 dB Bandwidth, FBW (GHz)	Gain at f_0 (dBi)
Step-1 with Full Ground $L_f = 28$ mm	2.40 4.83	−18.33 −18.99	5% (2.32–2.44) 8.07% (4.68–5.07)	2.63
Step-2 with Full Ground $L_f = 23$ mm	2.40 4.88	−16.60 −20.31	5% (2.30–2.42) 6.56% (4.72–5.04)	2.84
Step2-(Step-3 + Step-4) = Step-5	Not resonant	No S_{11} below −10 dB	No −10 dB bandwidth observed	−1.79
Step-5-Step-6 = Step-7	Not resonant	No S_{11} below −10 dB	No −10 dB bandwidth observed	−1.48
Step-8 with Substrate size $W_s = 59.70$ mm and Length, $L_s = 58.68$ mm	Not resonant	No S_{11} below −10 dB	No −10 dB bandwidth observed	1.66
Step-9 with compressed Substrate width $W_s = 53.68$ mm and length, $L_s = 58.68$ mm	Not resonant	No S_{11} below −10 dB	No −10 dB bandwidth observed	1.46
Step-10 compressed Substrate width, $W_s = 53.68$ mm and length, $L_s = 55$ mm	Not resonant	No S_{11} below −10 dB	No −10 dB bandwidth observed	1.63

* f_r = Resonating frequency; f_0 = design frequency; S_{11} = Reflection coefficient; FBW: Fractional bandwidth

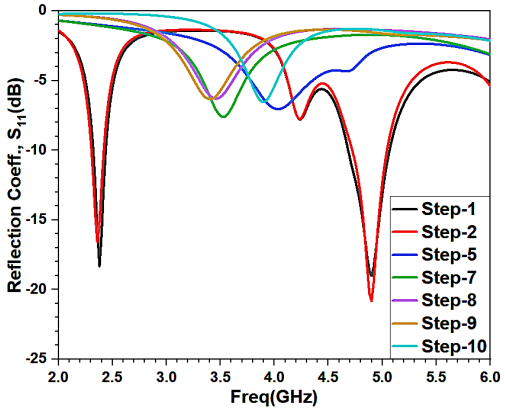

FIGURE 3. Effect of binary operations on a rectangular patch with full ground.

sections shown in Step 3 and Step 4 of Fig. 1 (highlighted in red and green) are subtracted from the rectangular patch obtained in Step 2, resulting in Step 5. In Step 5, the patch with a full bottom surface as the ground results in no significant results below −10 dB reflection coefficients, bandwidth, and gain values. Two symmetric regular octagons of side length equal to 15.307 mm, as displayed in Step 6, were subtracted from the patch in Step 5. This yields the patch geometry in Step 7. With this radiating patch in Step 7, no significant resultant parameters were obtained. To minimize the antenna size, first, the substrate and ground length is reduced to 53.68 mm (Steps 8 and 9). Again, no significant resultant parameter was obtained with these steps, except that the peak gain became positive. Furthermore, the feed length is reduced to 8.0 mm, and the antenna width is compressed to 53.68 mm (Step 10). Using this technique, a proposed lamp-shaped antenna patch was developed with a full bottom surface as the ground. Compression of the overall substrate ground length and width resulted in a positive gain. Fig. 3 depicts the reflection coefficients for each stage, and Table 2 lists the resulting parameters.

2.3. Variation of Ground Length

The full ground length on the bottom surface of the patched and sandwiched jeans substrate forms a capacitor. The capacitance of the capacitor depends on the ground area. As the length of the substrate decreased, the area between the patch and the ground also decreased; consequently, the capacitance decreased. This reduced area results in reduced current density across the patch. On the other hand, the capacitance near the feed and upper edge of the patch became dominant, which resulted in higher current density magnitudes. The truncated corners of the patch result in increased electrical length and, hence, improved low-frequency performance in the same manner as a quasi-fractal antenna [24]. Alternatively, a reduced ground length results in decreased capacitance and increased resonant frequency, which improves the high-frequency resonance. Another effect of the reduced ground length converts the antenna into a monopole-like behavior that results in improved dual-band performance.

Initially, the ground length of the compressed patch antenna in Step 10 was 100% ($L_g = 55$ mm), resulting in a gain of 1.63 dBi. Following that, the ground length was lowered to 50%, $L_g = 27.5$ mm, resulting in an antenna gain of 2.2 dBi rather than 1.63 dBi. The further reduction of ground length to 25% (i.e., $L_g = 13.75$ mm) results in the improvement of gain and attains a value of 4.08 dBi. All above-ground length reductions resulted in no significant values of the reflection coefficient below −10 dB; hence, no resonant frequency or −10 dB FBW was produced. Further reduction in the ground length below 25% ground (i.e., $L_g = 9.43$ mm) results in dual bands (2.17–2.86 GHz) and (4.52–5.06 GHz) with resonance frequencies at 2.45 GHz and 4.70 GHz. This results in a slight drop in gain at the design frequency ($f_0 = 2.45$ GHz), i.e., 3.86 dBi as opposed to the prior 4.08 dBi, while an exceptional gain of 6.63 dBi is attained at the second resonance frequency at 4.70 GHz. Fig. 4 compares the reflection coefficient and S_{11} plots of the reduced ground in all scenarios, and Table 3 shows the resulting parameter data.

TABLE 3. Effect of reduced ground.

Ground size	Tuning Freq. f_r (GHz)	S_{11} (dB)	−10 dB Bandwidth, FBW (GHz)	Gain dBi at f_0
Full (100%) ground ($L_g = 55$ mm)	Not resonant	No S_{11} below −10 dB	No −10 dB bandwidth observed	1.63
50% Reduced ground ($L_g = 27.50$ mm)	Not resonant	No S_{11} below −10 dB	No −10 dB bandwidth observed	3.83
25% Reduced ground ($L_g = 13.75$ mm)	Not resonant	No S_{11} below −10 dB	No −10 dB bandwidth observed	4.08
With Reduced ground ($L_g = 9.43$ mm)	2.45 4.70	−19.50 −13.34	28.16% (2.17–2.86) 13.62% (4.42–5.06)	3.86

* f_r = Resonating frequency; f_0 = design frequency; S_{11} = Reflection coefficient; FBW: Fractional bandwidth

TABLE 4. Antenna miniaturization.

Substrate size with Monopole Ground length $L_g = 9.43$ mm	Tuning Freq. f_r (GHz)	S_{11} (dB)	−10 dB Bandwidth FBW (GHz)	Gain at f_0 (dBi)
$W_s = 59.7$ mm and $L_s = 78.68$ mm	2.42 5.49	−25.18 −11.01	29.75% (2.12–2.84) 15.48% (5.09–5.94)	3.75
$W_s = 59.7$ mm and $L_s = 73.68$ mm	2.40 5.54	−25.22 −10.80	30% (2.11–2.83) 13.89% (5.19–5.96)	3.71
$W_s = 59.7$ mm and $L_s = 58.68$ mm	2.38 5.42	−25.17 −12.85	30.25% (2.09–2.81) 24.72% (4.84–6.18)	3.74
$W_s = 53.9$ mm and $L_s = 58.68$ mm	2.48 4.76	−19.45 −12.01	29.03% (2.18–2.90) 13.23% (4.52–5.15)	3.88
$W_s = 53.9$ mm and $L_s = 55$ mm	2.45 4.70	−19.50 −13.34	28.16% (2.17–2.86) 13.61% (4.42–5.06)	3.86

* f_r = Resonating frequency; f_0 = design frequency; S_{11} = Reflection coefficient; FBW: Fractional bandwidth

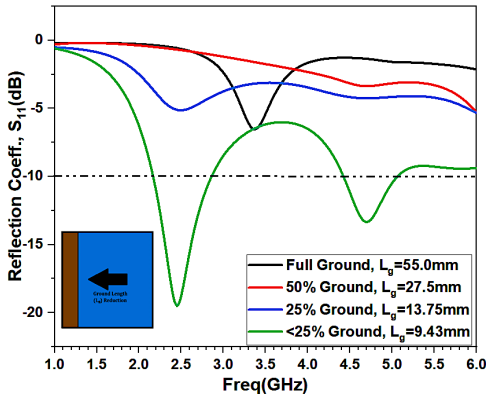

FIGURE 4. Effect of ground length reduction.

2.4. Substrate Size Miniaturization

The design begins with the feed length equal to a ¼ of the guided wavelength, i.e., $L_f = \frac{\lambda_g}{4} = 28$ mm and substrate size equal to $W_s \times L_s = 59.7$ mm $\times 78.68$ mm with ground length equal to 9.43 mm. This results in dual-band S_{11} performance below −10 dB at resonance frequencies of 2.42 GHz and 5.49 GHz. To miniaturize the antenna's overall size, the length of the feed was reduced to one-third of $\frac{\lambda_g}{4}$ i.e., $L_f = \frac{\lambda_g}{12} = 8$ mm, and the corresponding length of the substrate was reduced to 73.68 mm in length. In this case, the first resonance frequency shift was observed at 2.40 GHz, whereas the upper resonance frequency was noticed at 5.54 GHz with a small reduction in the gain value. Furthermore, the substrate length continues to reduce to 58.68 mm. In this scenario, the first resonance frequency shift occurred at 2.38 GHz, whereas the top resonance frequency was detected at 5.42 GHz with a slight increase in gain values. The antenna was squeezed across the breadth ($W_s = 53.9$ mm) while maintaining the same length ($L_s = 58.68$ mm). In this scenario, the first resonance frequency shift was recorded at 2.48 GHz, whereas the upper resonance frequency was detected at 4.76 GHz with an increase in gain. To achieve resonance at the design frequency, the substrate length is shortened to 55 mm, resulting in a first resonance frequency of 2.45 GHz, while the upper resonance frequency is 4.70 GHz with an increased gain value of 3.86 dBi. The total antenna size was reduced to 37.15% of the root rectangle patch antenna size (59.7 mm × 78.68 mm). Table 4 lists the resultant parameters for all miniaturization steps, and Fig. 5 illustrates their reflection coefficients.

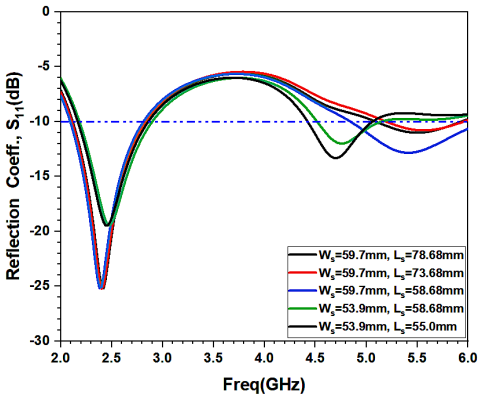

FIGURE 5. Effect of antenna size miniaturization.

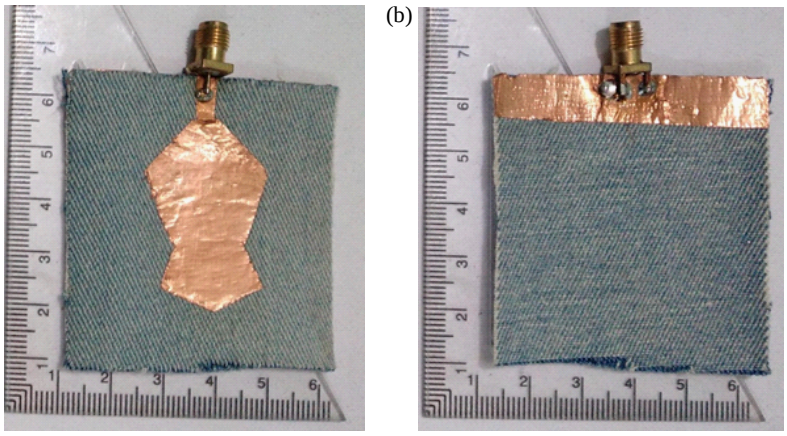

FIGURE 6. Fabricated antenna. (a) Front view, (b) rear view.

3. RESULTS AND DISCUSSIONS

3.1. Prototype of the Fabricated Antenna

First, an ABBE reflectometer was used to assess the permittivity of the jeans substrate. The antenna is made by pasting self-adhesive copper tape on the top and bottom layers of the same 53.9 mm × 55 mm jeans substrate. With the aid of the drawing file, the copper tape was cut with a sharp paper cutter in accordance with the antenna's optimized design dimensions, as shown in Fig. 2. Next, a 50 Ω SMA connector was soldered with caution using cloth burns and copper tape. Figs. 6(a) and 6(b) show the front and rear views of the antenna from the manufactured prototype model.

3.2. Substrate Dielectric Properties and Antenna Reflection Coefficients Measurements

First, the dielectric characteristics of the dry jeans substrate were examined using the R&S ZNB-20 Vector Network Analyzer (VNA) and Dielectric Assessment Kit (DAK)-3.5 probes over a frequency range of 2–6 GHz [28]. Dry jeans samples' dielectric permittivity, conductivity, and loss tangent are determined using the open-ended coaxial probe (OCP) method spanning 2–6 GHz frequency ranges. The measurement setup is shown in Fig. 7(a). The electromagnetic field propagates along the coaxial line and is reflected when the probe and Matterial Under Test (MUT) have different impedances. The vector network analyzer software converted the reflection data into dielectric parameters. The detected reflections (reflection coefficient S_{11}) were translated into dielectric characteristics. Complex permittivity analyses of the dielectric behavior under high-frequency electric fields are presented in this section. Equation (1) describes the complex permittivity of a material (ε^*):

$$\varepsilon^* = \varepsilon' + j\varepsilon'' \tag{1}$$

The dielectric constant of a material ($\varepsilon' = \varepsilon_r$) quantifies the energy stored by an external electric field, whereas the imaginary component of the complex permittivity (ε'') indicates the dissipative factor. A crucial factor in system loss is material conductivity ($\varepsilon'' = \frac{\sigma}{\omega}$), which converts electromagnetic energy into thermal energy. Larger imaginary parts wasted more energy. Equation (2) shows that the loss tangent affects the material efficacy.

$$\tan\delta = \frac{\varepsilon''}{\varepsilon'} = \frac{\sigma}{\omega\varepsilon'} \tag{2}$$

The efficiency of the microwave-to-thermal energy conversion is often measured using the loss tangent. Equation (2) states that the loss tangent is frequency dependent and proportional to the material conductivity. Equation (3) calculates the average material properties from 2–6 GHz. The Jeans substrate material under test (MUT) has an average dielectric constant, dielectric loss tangent, and conductivity of 1.60005, 0.050307, and 0.0523 S/m in all frequency ranges (2–6 GHz).

$$\text{Average substrate properties} = \frac{\sum\left(f_{2\,\text{GHz}} + f_{2.04\,\text{GHz}} + f_{2.08\,\text{GHz}} + \ldots + f_{6\,\text{GHz}}\right)}{101} \tag{3}$$

The simulated and measured reflection coefficient (S_{11}) curves are shown in Fig. 7(b). The simulated resonance frequencies on the graph are 2.45 GHz and 4.70 GHz. 28.16% and 11.49% are the −10 dB fractional bandwidths (FBW) in the simulated plot. −19.50 dB and −13.34 dB were the lowest reflection coefficient values at these frequencies. The measured reflection coefficients resemble the calculated (S_{11}) figure, with somewhat broader bandwidths in both the lower and upper bands. Soldering of 50 Ω SMA connector connections, connection losses, fabrication faults, tolerances in dimensions, and variances in practically accessible substrate qualities are the main causes of these disparities.

3.3. *E*-Plane and *H*-Plane Radiation Patterns of the Proposed Antenna

Figures 8(a)–(b) shows the similarity between the measured and simulated E-plane and H-plane gain radiation patterns of the antenna at resonance frequencies of 2.45 GHz and 4.70 GHz. The gain radiation patterns were bidirectional in both the E- and H-planes. The radiation patterns in three dimensions at two resonance frequencies are shown in Figs. 8(c)–(d). The gain values displayed in these figures are in dB. The peak gain values

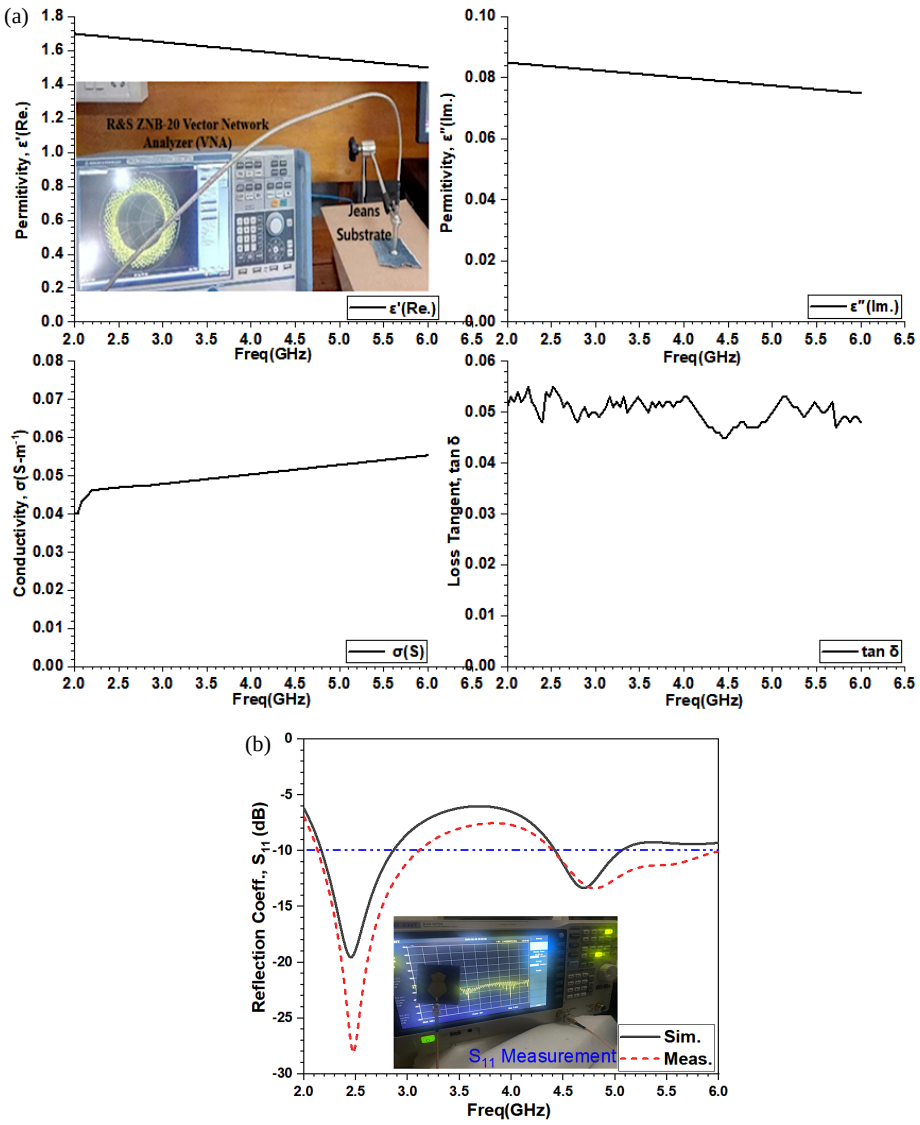

FIGURE 7. Substrate and antenna measurements. (a) Substrate dielectric properties, and (b) simulated and measured (S_{11}).

at these two resonating frequencies, 2.45 GHz and 4.70 GHz, in the figures are 3.86 dBi and 6.63 dBi, respectively. The gain of the reference isotropic (a theoretical point source that radiates equally in all directions) is 2.15 dBi.

3.4. Antenna Gain and Axial Ratio

An anechoic chamber (up to 30 GHz) was used to measure the gain of the jeans lamp-shaped fabric antenna (AUT). A double-ridge pyramidal horn antenna was used as the reference antenna. The distance between the reference horn antenna and the antenna under test (AUT) was 30 cm (made greater than 49.4 mm, i.e., $> 2D^2\lambda$ to maintain the far-field condition, where D is the large dimension of the jeans antenna, i.e., 55 mm). The antenna gain was measured in an anechoic chamber by using a comparison method with a calibrated horn antenna. After satisfying the far-field condition and performing VNA calibration, the reference antenna was replaced by the AUT. Fig. 9 depicts the simulated and measured antenna gain plots and the antenna gain measurement setup in the anechoic chamber. The simulated peak gain value at 4.825 GHz was found to be 7.09 dBi. At the two resonance frequencies, the values are 3.86 dBi and 6.63 dBi. These gain values are 2.15 dB higher than those appear in Fig. 8(c) and Fig. 8(d). At these frequencies, the antenna had radiation efficiencies of 96.34% and 92.27%, respectively. The measured gain matched the simulated gain, validating the antenna gain performance. The axial ratio elaborates on the orientation of the electric or magnetic field vector; in other words, the polarization information is hidden inside the axial ratio graph. If the axial ratio is less than 3 dB, the antenna is circularly polarized; for higher axial ratios, the polarization is linear. Fig. 10 shows the axial ratio map of the proposed antenna. The graph shows that all the axial ratio values are more than 3 dB, indicating that the planned antenna is linearly polarized.

3.5. Surface Current Distribution

The magnitude of the surface current distribution of the antenna is shown in Figs. 11(a)–(c). The surface current on a conven-

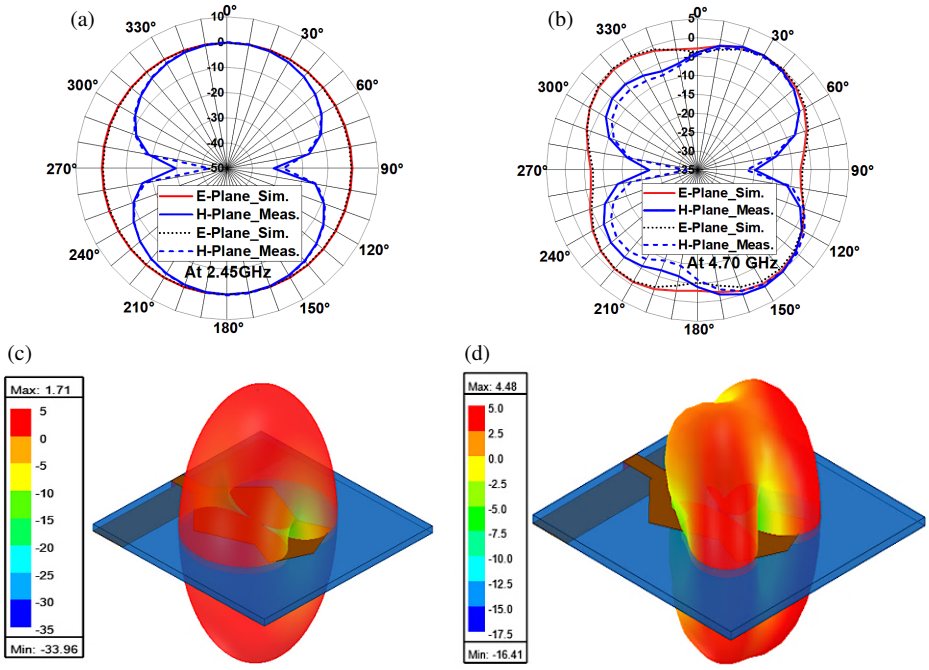

FIGURE 8. Antenna radiation pattern plots. (a) E-plane, and H-plane at 2.45 GHz, (b) E-plane, and H-plane at 4.70 GHz, (c) 3D-view at 2.45 GHz (gain values are in dB), and (d) 3D-view at 4.70 GHz (gain values are in dB).

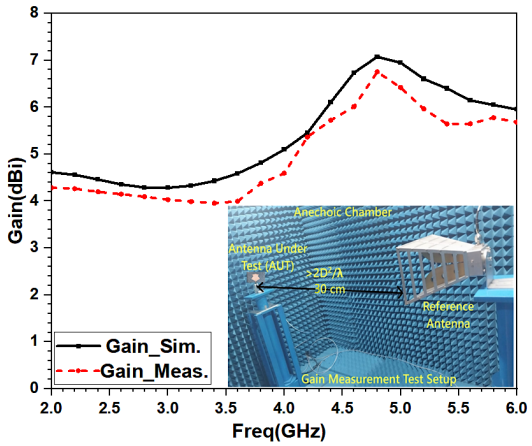

FIGURE 9. Simulated and measured gains.

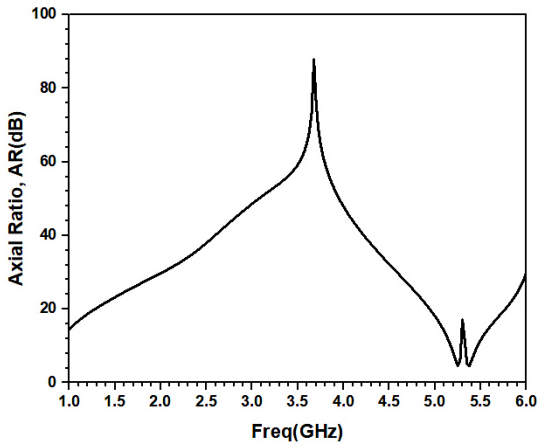

FIGURE 10. Simulated axial ratio.

tional rectangular patch was very small in magnitude, as shown in Fig. 11(a). Then, four right-angled triangular cuts were removed from the corners of the rectangular patch, and the antenna became diamond-shaped. The magnitude of the current in the diamond-shaped antenna is shown in Fig. 11(b). This operation improves the magnitude of the current distribution in the patch. To further alter the current distribution, two regular octagons with an edge length of 15.307 mm were cut by taking the centers of the diamond-shaped corners. This increased the total electrical length and resulted in a lamp-shaped antenna. The magnitude of the current distribution is shown in Fig. 11(c).

3.6. RLC Electrical Equivalent Circuit of the Lamp-Shaped Wearable Antenna

The RLC equivalent circuit captures the input impedance behavior of an antenna across its working band. Assigning the radiating structure to a resistor (R), inductor (L), or capacitor (C) allows designers to treat the antenna as a passive component in a microwave network. The series/parallel combination indicates whether the antenna is capacitive or inductive at a given frequency, influencing the network architecture selection (e.g., compensating for excess capacitance using a shunt inductor). The quality factor (Q) is directly related to the fractional bandwidth. A lower Q indicates a broader bandwidth; the trading size for the bandwidth is possible by adjusting L or C. The resistor represents the radiation loss. The efficiency can be determined without full-wave simulations by comparing it with the material loss resistance. By mapping the circuit parts to physical features, for example, patch length (C) and feed-line inductance (L), it is possible to alter the geometry predictably to achieve the desired resonance. The corresponding circuit can be entered into circuit simulators Advanced Design Software

TABLE 5. The RLC equivalent circuit's passive component values.

Frequency, f_r (GHz)	R, L, and C Passive Component	R, L, and C Passive Component Value
First Resonating Frequency, $f_r = 2.45$ GHz (Series resonating circuit in shunt arm)	R_1	63.5544 Ω
	L_1	16.73628 nH
	C_1	0.26571 pF
Non-Resonating Frequency, $f_r = 3.72$ GHz (Shunt resonating circuit in the series arm)	R_2	284.6688 Ω
	L_2	1.07446 nH
	C_2	0.49487 pF
Second Resonating Frequency, $f_r = 4.70$ GHz (Series resonating circuit in shunt arm)	R_3	62.564 Ω
	L_3	0.2664 nH
	C_3	0.39375 pF

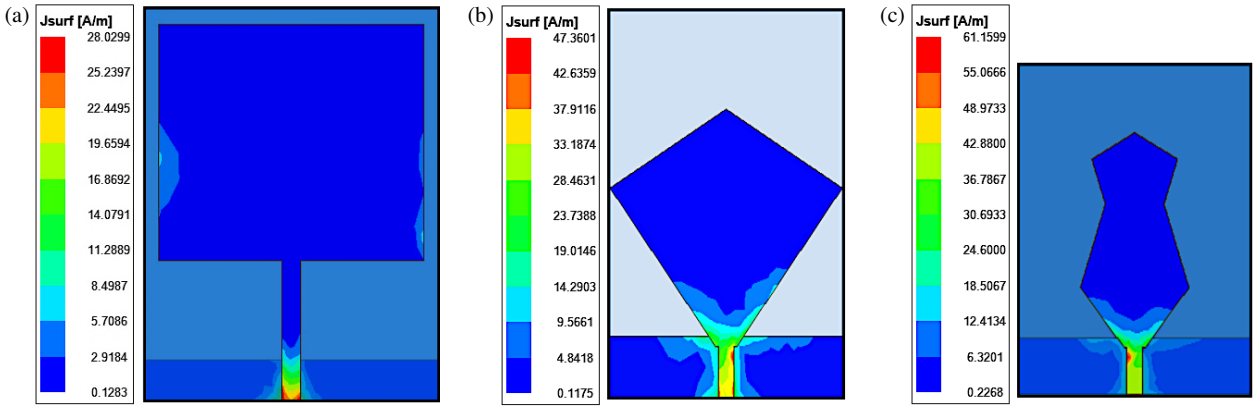

FIGURE 11. Surface current distribution of antenna at 2.45 GHz. (a) Rectangular patch, (b) diamond-shaped, and (c) lamp-shaped.

(ADS, Keysight Genesys, etc.) to investigate the antenna, front-end RF blocks, power amplifier stability, and filter interactions.

An RLC electrical equivalent circuit was generated using the bandwidth and resonance frequencies from the reflection coefficient plot of the lamp-shaped dual-band wearable antenna. The two resonating frequencies, 2.45 GHz and 4.70 GHz, produce two series resonating circuits in the shunt branch. There is one non-resonating frequency, 3.72 GHz, which corresponds to an extreme reflection coefficient. This resulted in a parallel resonating circuit in the series branch, as illustrated in Fig. 12(a). The values of R, L, and C were calculated using the typical series and parallel resonance circuit relationships [18, 29–33]. The estimated tuned R, L, and C values are presented in Table 5. The circuit is simulated using an Advanced Design System (ADS) and confirmed by comparing the constructed wearable antenna reflection coefficient with the equivalent tuned circuit in the ADS (Fig. 12(b)) [31, 32]. The two reflection coefficients agreed well with each other. The R, L, and C tolerances of the passive components affect the bandwidth of the ADS circuit reflection coefficients.

3.7. ON-Body and OFF-Body SAR Investigation

The phantom model proposed at the top right of Fig. 13(a) has skin, fat, and muscle for body analysis of the antenna, and the targeted layer has its own properties, as shown in the table. A three-layered human body phantom was formed based on the standard phantom model values [25, 34, 35]. These layers were placed over one another to form the human phantom in the CST design environment, and the proposed antenna was placed over the phantom, as shown in the bottom left of Fig. 13(a). The antenna was then analyzed for SAR value calculation, and the resultant values were observed well under the specified limits. According to the ICNIRP guidelines, the SAR limit is 1.6 W/kg for 1 g of human tissue for distances less than 5.0 mm from the body phantom. The regulatory bodies that describe the limits for SAR are the Federal Communications Commission (FCC) of the US, the European Union (EU), and Innovation, Science and Economic Development (ISED) of Canada, which describe the standard regulations for SAR testing and SAR limits, thereby limiting emissions from RF devices for ON-body wireless transmissions. The SAR values of the proposed antenna are shown in Table 6, and these antenna SAR values are within the permissible limits recommended by the ICNIRP. The antenna is first mounted over the phantom model and then placed at 0 mm (ON-body), 2.0 mm (OFF-body summer dresses), and 5.0 mm (OFF-body winter dresses) from the phantom as shown in Figs. 13(b)–(d).

Figures 13(b)–(d) show the various SAR values obtained when the antenna was placed on the body phantom just in proximity (ON-body) in such a way that there was no distance

TABLE 6. SAR values of the antenna.

Proposed Antenna Distance from phantom	SAR Values				
	f-2.45 GHz	f-3.0 GHz	f-3.5 GHz	f-4.0 GHz	f-4.7 GHz
0 mm	0.905 W/Kg	1.5 W/Kg	1.28 W/Kg	0.855 W/Kg	0.592 W/Kg
2 mm	0.499 W/Kg	0.722 W/Kg	1.13 W/Kg	1.25 W/Kg	1.3 W/Kg
5 mm	0.421 W/Kg	0.679 W/Kg	0.946 W/Kg	0.912 W/kg	0.781 W/kg

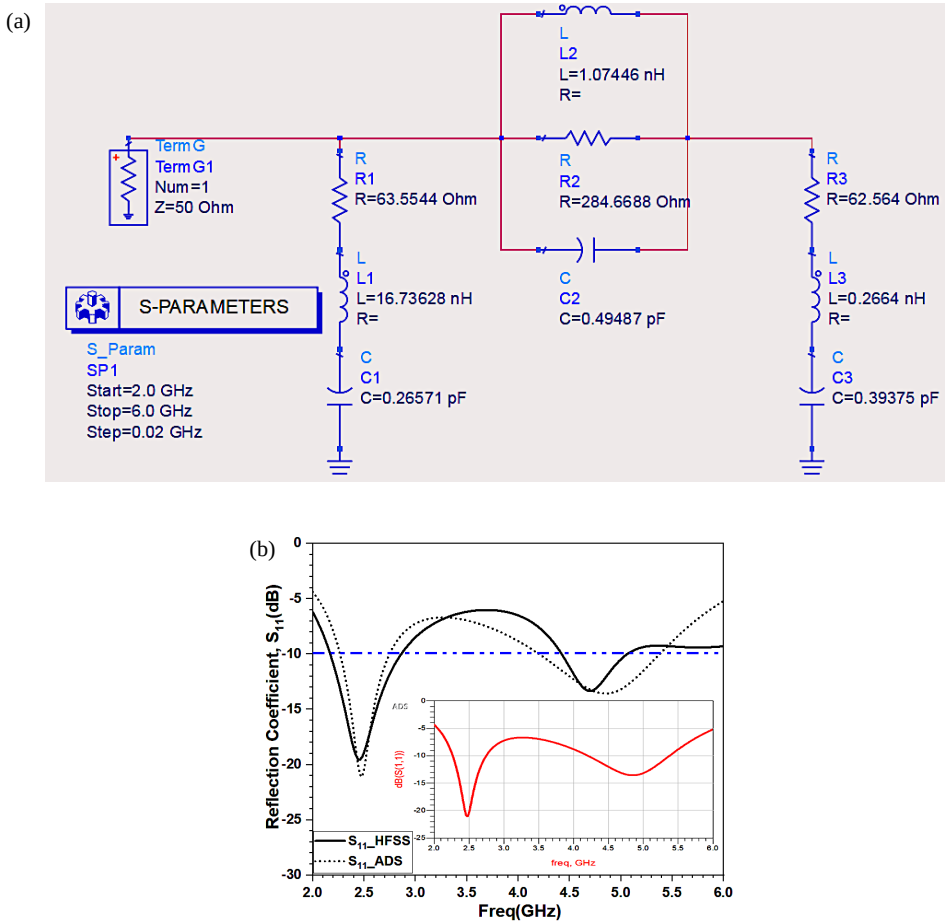

FIGURE 12. Equivalent circuit modelling. (a) RLC equivalent circuit, and (b) designed lamp-shaped antenna and generated RLC equivalent circuit reflection coefficients.

between the antenna and human phantom, and the SAR values were 0.905 W/kg, 0.592 W/Kg at 2.45 GHz, and 4.70 GHz. Similarly, when the antenna was placed at 2.0 mm from the body phantom (OFF-body with summer dresses), the SAR values obtained were 0.499 W/kg and 1.3 W/Kg at 2.45 GHz and 4.70 GHz. When the antenna was placed at a distance of 5.0 mm from the human body phantom (OFF-body with winter dresses), then the SAR values obtained were 0.421 W/Kg and 0.781 W/Kg at 2.45 GHz and 4.70 GHz, respectively. In all cases, the proposed antenna absorption levels remain within the acceptable limits specified by the relevant international regulatory authorities [39].

3.8. Resultant Parameters of the Proposed Antenna

The derived parameters of the proposed antenna are consolidated in Table 7.

3.9. Performance Comparison of Similarly Existing Antennas

The suggested design's comparisons with previously published works of a similar type and design, operating at approximately the same frequency of 2.45 GHz, are presented in Table 8, including antenna performance metrics. The comparison table indicates that the substrate with diminished permittivity and reduced thickness sustains a gain of over 5 dBi, exhibiting an en-

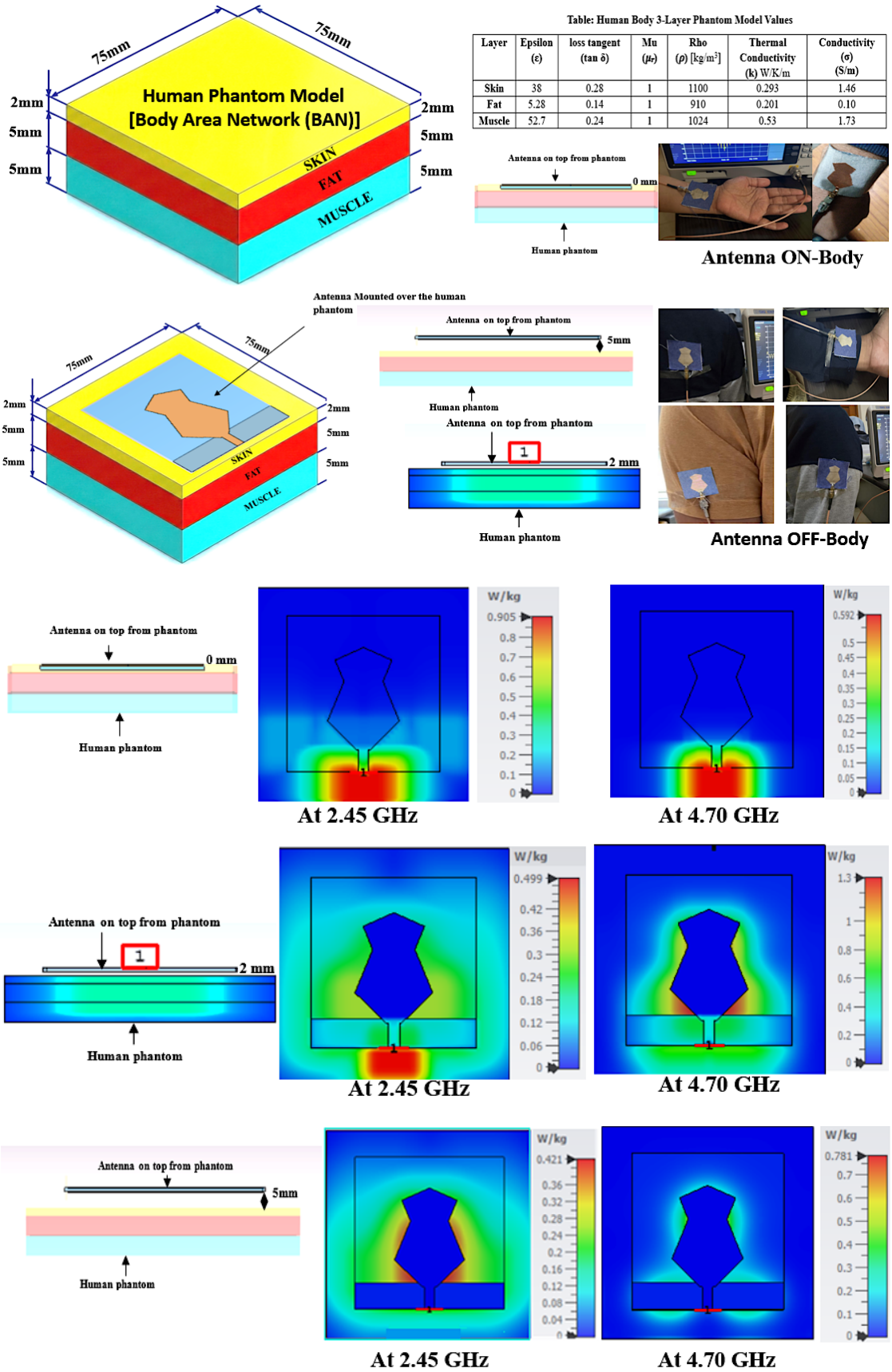

FIGURE 13. ON-body and OFF-body SAR investigation. (a) Phantom model, layer properties, real-time deployment of antenna on human body at different locations, (b) SAR value when antenna is placed on phantom at 0 mm, (c) SAR value of proposed antenna when placed at 2.0 mm, and (d)SAR value of proposed antenna when placed at 5.0 mm.

TABLE 7. The resultant parameters of the antenna.

Antenna Parameter	Simulated	
Resonant Frequency, f_r (GHz)	2.45	4.70
Reflection Coefficients, S_{11}(dB)	−19.50	−13.34
−10 dB Fractional Bandwidth, (GHz)	(2.17–2.86)	(4.42–5.06)
Fractional Bandwidth (FBW)	28.16%	13.61%
Polarization Type	Linear (AR > 3 dB)	Linear (AR > 3 dB)
Peak Gain (dBi) at f_r GHz	3.86	6.63
Radiation efficiency at 2.45 GHz	96.34%	92.27%
SAR (ON-body human phantom for 1 g tissue)	0.905 W/Kg	0.592 W/Kg
SAR (OFF-body human phantom for 1 g tissue) 2.0 mm distance	0.499 W/Kg	1.3 W/Kg
SAR (OFF-body human phantom for 1 g tissue) 5.0 mm distance	0.421 W/Kg	0.781W/kg

TABLE 8. Comparison with existing literature antennas.

Ref.	Ant. Shape and Feed Type	Substrate used	−10 dB BW (GHz)	f_r (GHz)	G (dBi)	Size (mm^3)	Ground	Rad. Eff. at f_r
[20] 2014	Rectangular patch inset-fed	Jeans ($\varepsilon_r = 1.6$)	2.40–2.50	2.492	9.41	120 × 120 × 1.6	Monopole	NG
[21] 2018	dual-band textile wearable antenna, coax-fed	Denim ($\varepsilon_r = 1.54$)	2.42–2.484 5.725–5.85	2.45 5.80	8.49 6.85	46 × 16 × 1.6	Monopole	NG
[22] 2020	Meandered structure, rectangular-shaped monopole, edge-fed	Polydimethylsiloxane (PDMS) ($\varepsilon_r = 2.71$)	2.40–2.50	2.45	4.04	30 × 33 × 1.0	Monopole	92%
[25]	Rectangular patch, tappered-fed	FR-4 ($\varepsilon_r = 4.4$)	2.30–4.125	2.48	5.80	34 × 28 × 1.58	Monopole with stub	NG
[36] 2019	Corner notched, rectangular slot monopole, edge-fed	semi-flexible, Rogers Duroid RO3003 ($\varepsilon_r = 3$)	1.95–2.65	2.45	NG	24 × 16 × 1.52	Monopole	NG
[37] 2021	L-slotted, L-shaped monopole, edge-fed	Semi-flexible, Rogers Duroid RO3003 ($\varepsilon_r = 3$)	2.35–2.60 5.70–5.86	2.45 5.80	NG	30 × 38 × 1.52	Compressed, Monopole	NG
[38] 2023	Rectangular patch monopole, edge-fed	Jeans ($\varepsilon_r = 1.6$)	2.0–3.15	2.40	NG	73 × 60 × 1.0	Compressed, Monopole	NG
This work	Lamp-shaped monopole, edge-fed	Jeans ($\varepsilon_r = 1.6$)	2.17–2.86 4.42–5.06	2.45 4.70	3.86 6.63	53.9 × 55 × 1.0	Monopole	96.34% 92.27%

*NG: Not Given; G: Antenna Gain.

hanced −10 dB fractional bandwidth, while the suggested dual-band antenna encompasses both the public safety band and the ISM band.

4. CONCLUSIONS

A wearable antenna was designed and tested satisfactorily. The simulated and measured findings were closely aligned. The antenna attains a maximum gain of 7.09 dBi at 4.825 GHz, with dual-wideband reflection coefficients and fractional bandwidths below −10 dB of 28.16% and 11.49%, respectively, and efficiencies above 92%. The proposed manufactured antenna is 37.15% smaller than a conventional patch antenna. The proposed antenna design features a triangular substrate length that regulates the resonance frequency. The generated RLC equivalent circuit of the antenna is beneficial for the antenna designer for system-level analysis. The SAR values of the antenna were investigated on the three-layered human phantom at various close distances, and these values were found suitable for the deployment in ON-body and OFF-body medical applications under ICNIRP, FCC, European Union (EU), ISED, and DoT standard guidelines. The proposed antenna is optimal for low-power MMIC/MIC transmitters and receivers utilized in Wi-Fi, WLAN, Wi-MAX, Bluetooth, public safety, rescue operations, concealed object detection, radar, military applications, and energy-harvesting devices. The proposed design has the potential to evolve into antennas featuring multiple inputs and outputs (MIMO) and multi-element arrays in the future. An identical antenna may be employed for human-oriented medical applications by accurately assessing the specific absorption rate (SAR) and bending effect.

ACKNOWLEDGEMENT

The authors would like to thank the Gurukula Kangri (deemed to be University), India, Universiti Teknikal Malaysia Melaka (UTeM), the Center of Research and Innovation Management (CRIM), and the Ministry of Higher Education (MOHE) of Malaysia for supporting this project.

REFERENCES

[1] Al-Gburi, A. J. A., N. H. M. Radi, T. Saeidi, N. J. Mohammed, Z. Zakaria, G. S. Das, A. Buragohain, and M. M. Ismail, "Superconductive and flexible antenna based on a tri-nanocomposite of graphene nanoplatelets, silver, and copper for wearable electronic devices," *Journal of Science: Advanced Materials and Devices*, Vol. 9, No. 3, 100773, 2024.

[2] Kennedy, T. F., P. W. Fink, A. W. Chu, N. J. Champagne, G. Y. Lin, and M. A. Khayat, "Body-worn E-textile antennas: The good, the low-mass, and the conformal," *IEEE Transactions on Antennas and Propagation*, Vol. 57, No. 4, 910–918, 2009.

[3] Bai, Q. and R. Langley, "Crumpling of PIFA textile antenna," *IEEE Transactions on Antennas and Propagation*, Vol. 60, No. 1, 63–70, 2012.

[4] Al-Gburi, A. J. A., I. Ibrahim, Z. Zakaria, and A. D. Khaleel, "Bandwidth and gain enhancement of ultra-wideband monopole antenna using MEBG structure," *ARPN Journal of Engineering and Applied Sciences (JEAS)*, Vol. 14, 3390–3393, 2019.

[5] Huang, J.-S., T.-Y. Jiang, Z.-X. Wang, S.-W. Wu, and Y.-S. Chen, "A novel textile antenna using composite multifilament conductive threads for smart clothing applications," *Microwave and Optical Technology Letters*, Vol. 58, No. 5, 1232–1236, 2016.

[6] Hu, X., S. Yan, and G. A. E. Vandenbosch, "Wearable button antenna for dual-band WLAN applications with combined on and off-body radiation patterns," *IEEE Transactions on Antennas and Propagation*, Vol. 65, No. 3, 1384–1387, 2017.

[7] Agneessens, S., S. Lemey, T. Vervust, and H. Rogier, "Wearable, small, and robust: The circular quarter-mode textile antenna," *IEEE Antennas and Wireless Propagation Letters*, Vol. 14, 1482–1485, 2015.

[8] Al-Gburi, A. J. A., M. M. Ismail, N. J. Mohammed, A. Buragohain, and K. Alhassoon, "Electrical conductivity and morphological observation of hybrid filler: Silver-graphene oxide nanocomposites for wearable antenna," *Optical Materials*, Vol. 148, 114882, 2024.

[9] Hariharasudhan, K. and R. Kumari, "Metasurface loaded patch antenna for Wi-Fi applications," in *2019 TEQIP III Sponsored International Conference on Microwave Integrated Circuits, Photonics and Wireless Networks (IMICPW)*, 321–323, Tiruchirappalli, India, 2019.

[10] Karimah, S., F. Y. Zulkifli, Basari, and E. T. Rahardjo, "Antenna design for femtocell LTE at frequency 2.3–2.4 GHz," in *2014 Makassar International Conference on Electrical Engineering and Informatics (MICEEI)*, 50–53, Makassar, Indonesia, 2014.

[11] Saravanan, M. and M. J. S. Rangachar, "A narrowband corner slot patch antenna for 2.4 GHz wireless radio communications," *International Journal of Engineering and Technology*, Vol. 8, No. 5, 2149–2153, 2016.

[12] Palandöken, M., C. Baytöre, and A. Kaya, "Compact WLAN monopole antenna with L-shaped strip line and spiral line loaded ring resonator," in *Proceedings of the 2nd World Congress on Electrical Engineering and Computer Systems and Science (EECSS'16)*, EEE 139–1–EEE 139–6, Budapest, Hungary, 2016.

[13] Yadav, N. P., "A four element antenna array for amateur radio applications," *National Journal of Antennas and Propagation*, Vol. 1, No. 1, 13–16, 2019.

[14] Al-Gburi, A. J. A., M. M. Ismail, N. J. Mohammed, and T. A. H. Alghamdi, "SAR flexible antenna advancements: Highly conductive polymer–graphene oxide–silver nanocomposites," *Progress In Electromagnetics Research M*, Vol. 127, 23–30, 2024.

[15] Balanis, C. A., *Antenna Theory: Analysis and Design*, 2nd ed., John Wiley & Sons, 1997.

[16] Nurhayati, N., A. N. D. N. Fahmi, P. Puspitaningayu, O. Wiriawan, B. Raafi'u, F. A. Iskandarianto, A. J. A. Al-Gburi, A. K. Varshney, and S. Johari, "Wearable wideband textile coplanar Vivaldi antenna for medical and IoT application," *Progress In Electromagnetics Research C*, Vol. 148, 145–156, 2024.

[17] Varshney, A., V. Sharma, T. M. Neebha, and N. P. Kumari, "Notch-band eliminator wideband CSRR loaded monopole fractal antenna for ISM and PCS communications," *World Journal of Engineering*, Vol. 21, No. 4, 821–834, 2024.

[18] Varshney, A., N. Cholake, and V. Sharma, "Low-cost ELC-UWB fan-shaped antenna using parasitic SRR triplet for ISM band and PCS applications," *International Journal of Electronics Letters*, Vol. 10, No. 4, 391–402, 2022.

[19] Varshney, A., T. M. Neebha, V. Sharma, J. G. Jency, and A. D. Andrushia, "Dodecagon-shaped frequency reconfigurable antenna practically loaded with 3-delta structures for ISM band and wireless applications," *IETE Journal of Research*, Vol. 69, No. 11, 7747–7759, 2023.

[20] Purohit, S. and F. Raval, "Wearable-textile patch antenna using jeans as substrate at 2.45 GHz," *International Journal of Engineering Research & Technology (IJERT)*, Vol. 3, No. 5, 2456–2460, 2014.

[21] Wang, K.-H. and J.-S. Li, "Jeans textile antenna for smart wearable antenna," in *2018 12th International Symposium on Antennas, Propagation and EM Theory (ISAPE)*, 1–3, Hangzhou, China, 2018.

[22] Zerith M., A. T. and M. Nesasudha, "A compact wearable 2.45 GHz antenna for WBAN applications," in *2020 5th International Conference on Devices, Circuits and Systems (ICDCS)*, 184–187, Coimbatore, India, 2020.

[23] Singer, A., "Applications and antenna selection in the 4.9 GHz band," *Microwave Journal*, Vol. 50, No. 10, 136–144, 2007.

[24] Varshney, A., "High-gain miniaturized reduced electrical length circular quasi-fractal antenna for U-band and mm-wave (5G-advanced and 6G) communications," *Discover Electronics*, Vol. 2, No. 1, 90, 2025.

[25] Zebiri, C., S. Mekki, D. Sayad, I. Elfergani, M. L. Bouknia, R. Zegadi, A. Varshney, and J. Rodriguez, "Low SAR-UWB rectangular microstrip magnetic monopole antenna for S-band and biomedical applications," *Applied Computational Electromagnetics Society Journal (ACES)*, Vol. 40, No. 3, 212–225, 2025.

[26] Ouyang, Y. and W. J. Chappell, "High frequency properties of electro-textiles for wearable antenna applications," *IEEE Transactions on Antennas and Propagation*, Vol. 56, No. 2, 381–389, 2008.

[27] Yang, L., L. J. Martin, D. Staiculescu, C. P. Wong, and M. M. Tentzeris, "Conformal magnetic composite RFID for wearable RF and bio-monitoring applications," *IEEE Transactions on Microwave Theory and Techniques*, Vol. 56, No. 12, 3223–3230, 2008.

[28] Roy, S., S. Ghosh, S. S. Pattanayak, and U. Chakarborty, "Dual-polarized textile-based two/four element MIMO antenna

with improved isolation for dual wideband application," *International Journal of RF and Microwave Computer-Aided Engineering*, Vol. 30, No. 9, e22292, May 2020.

[29] Thereja, B. L., "Basic electrical engineering," *Electrical Technology*, Vol. 1, TMH, 2020.

[30] Varshney, A., D. N. Genccodhlan, I. Elfergani, J. Rodriguez, C. Zebiri, and T. M. Neebha, "Characterizations of effective parameters and circuit modeling of U-coupled hybrid ring resonator band pass filter," *IEEE Access*, Vol. 13, 2529–2545, 2024.

[31] Varshney, A., V. Sharma, and A. Srivastava, "A novel simplified equivalent modeling method for microstrip line interconnects," Indian Patent-202111019468, 2021.

[32] Varshney, A., V. Sharma, I. Elfergani, C. Zebiri, Z. Vujicic, and J. Rodriguez, "An inline V-band WR-15 transition using antipodal dipole antenna as RF energy launcher @ 60 GHz for satellite applications," *Electronics*, Vol. 11, No. 23, 3860, 2022.

[33] Varshney, A., "Novel mutually-coupled with microstrip glass fed circular ring antenna for Wi-Fi WLAN and ISM band applications," *International Journal of Electronics Letters*, Vol. 13, No. 3, 331–347, 2025.

[34] Duan, Z., Y.-X. Guo, R.-F. Xue, M. Je, and D.-L. Kwong, "Differentially fed dual-band implantable antenna for biomedical applications," *IEEE Transactions on Antennas and Propagation*, Vol. 60, No. 12, 5587–5595, 2012.

[35] Gabriel, S., R. W. Lau, and C. Gabriel, "The dielectric properties of biological tissues: III. Parametric models for the dielectric spectrum of tissues," *Physics in Medicine & Biology*, Vol. 41, No. 11, 2271, 1996.

[36] Shah, S. M., N. F. A. Kadir, Z. Z. Abidin, F. C. Seman, S. A. Hamzah, and N. Katiran, "A 2.45 GHz semi-flexible wearable antenna for industrial, scientific and medical band applications," *Indonesian Journal of Electrical Engineering and Computer Science*, Vol. 15, No. 2, 814–822, 2019.

[37] Shah, S. M., A. A. Rosman, M. A. Z. A. Rashid, Z. Z. Abidin, F. C. Seman, H. A. Majid, S. H. Dahlan, S. A. Hamzah, N. Katiran, A. Ponniran, F. Hassan, and F. Zubir, "A compact dual-band semi-flexible antenna at 2.45 GHz and 5.8 GHz for wearable applications," *Bulletin of Electrical Engineering and Informatics*, Vol. 10, No. 3, 1739–1746, 2021.

[38] Ghodake, A. and B. Hogade, "ISM band 2.4 GHz wearable textile antenna for glucose level monitoring," *International Journal of Electrical and Electronics Research (IJEER)*, Vol. 11, No. 1, 39–43, 2023.

[39] Mukherjee, N., A. Kundu, B. Gupta, and M. Mitra, "Specific absorption rate estimation for a typical hibiscus flower model as per ICNIRP electromagnetic guidelines," in *2020 IEEE Calcutta Conference (CALCON)*, 240–243, Kolkata, India, 2020.